Graphite to Diamond: Origin for Kinetics Selectivity

Yao-Ping Xie,[†,‡] Xiao-Jie Zhang,[†] and Zhi-Pan Liu*,[†]

[†]Collaborative Innovation Center of Chemistry for Energy Material, Shanghai Key Laboratory of Molecular Catalysis and Innovative Materials, Key Laboratory of Computational Physical Science, Department of Chemistry, Fudan University, Shanghai 200433, China

[‡]Key Laboratory for Microstructures, School of Materials Science and Engineering, Shanghai University, Shanghai 200072, China

S *Supporting Information*

ABSTRACT: Under mild static compression (15 GPa), graphite preferentially turns into hexagonal diamond, not cubic diamond, the selectivity of which is against thermodynamics. Here we, via novel potential energy surface global exploration, report seven types low energy intermediate structures at the atomic level that are key to the kinetics of graphite to diamond solid phase transition. On the basis of quantitative kinetics data, we show that hexagonal diamond has a facile initial nucleation mechanism inside graphite matrix and faster propagation kinetics owing to the presence of three coherent graphite/hexagonal diamond interfaces, forming coherent nuclei in graphite matrix. By contrast, for the lack of coherent nucleus core, the growth of cubic diamond is at least 40 times slower and its growth is inevitably mixing with that of hexagonal diamond.

It has long been a dream to manufacture large diamond crystals from graphite (G).[1−4] Modern research shows that cubic diamond (CD), despite most thermodynamically stable among carbon allotropes above ∼5 GPa, is not the main product under mild static compression of graphite, ∼15 GPa and ∼1000 °C[4−7] (The T∼P phase diagram of carbon is shown in Supporting Information, SI). The prevalence of heterophase junctions and the dominance of hexagonal diamond (HD) product are obstacles toward the growth of large diamond crystals. How to reduce the reaction pressure and control the selectivity of solid phase transition must rank one of the top challenges in material science. Extensive fundamental studies have been conducted in past decades to understand the diamond phase growth, but the kinetics data computed from theory are still at odds with general experimental findings.[8−13] How diamonds emerge from graphite is largely elusive.

The graphite phase transition to diamond as a typical diffusionless transition,[14] is governed by nucleation−growth mechanism under low pressures (<20 GPa).[6,10] Similar to many other diffusionless transitions, the morphology and interfacial structure of nucleation core are difficult to characterize due to the rapid and local atomic restructuring in phase transition once the reaction condition is reached. The interface of nucleation core is particularly important at the initial stage of nucleation since it dominates the thermodynamic stability of the nascent core. The quantitative determination of the structure and the stability of the interfaces are essential for establishing the kinetics, which, however, are still out of reach from both theory and experiment, not least because of the corrugated and multidimensional potential energy surface (PES) of carbon solid phase transition. For the lack of knowledge on the diamond nuclei, current theoretical simulations fail in general to predict correctly the pressurization product of graphite. These include first-principles total energy pathway calculations,[8,15] constant-pressure molecular dynamics (MD),[9] which found that, in contrast with experiment, CD should be the favored product under low pressures (<20 GPa), where the phase transition is assumed to follow a homogeneous (concerted) mechanism. Even with the nucleation mechanism by assuming the interfaces from concerted mechanism, the barrier to form CD nuclei is still lower than that to form HD nuclei, suggesting the importance to characterize the nuclei and their interface structures.

Here we utilize novel theoretical tools, namely stochastic surface walking (SSW) global optimization[16] and SSW reaction pathway sampling,[17] to resolve the anisotropic growth pathways of the graphite-to-diamond phase transition under 15 GPa. These new methods allow, for the first time, the highly corrugated PES of carbon phases being sampled extensively and unbiasedly, which leads to the identification of all transient heterophase junctions, which form the interfaces between diamond nuclei and graphite. The transition states (TS) are determined accurately for the junction-mediated pathways and the barrier height of diamond formation are computed. The kinetics not only rationalizes why HD is preferentially produced but also predicts that CD domain is always interwoven with HD domain in phase propagation at elevated temperatures.

Our SSW global PES exploration was utilized first to scan the phase space of carbon allotropes. Different from the conventional structure prediction where the global minimum is aimed, we here look for those less stable, less ordered heterophase junctions that are transient in kinetics. Although such tasks were often formidable using MD simulation, the SSW method developed recently is designed to explore complex PES efficiently via smooth surface walking along softened modes.[16−18] (All simulation details concerning SSW methodology and pathway sampling are described in SI). Our SSW simulations were carried out in a series of supercells up to 32-atom per cell at 15 GPa until no more types of junctions were revealed from PES exploration (>10^6 minima collected). The interaction of carbon is described by the environment dependent interatomic potential (EDIP)[19] that was found to describe well the major low energy carbon allotropes.

In total, more than 4000 minima were identified that are distinct from graphite and have relative low energetics (0.3 eV per
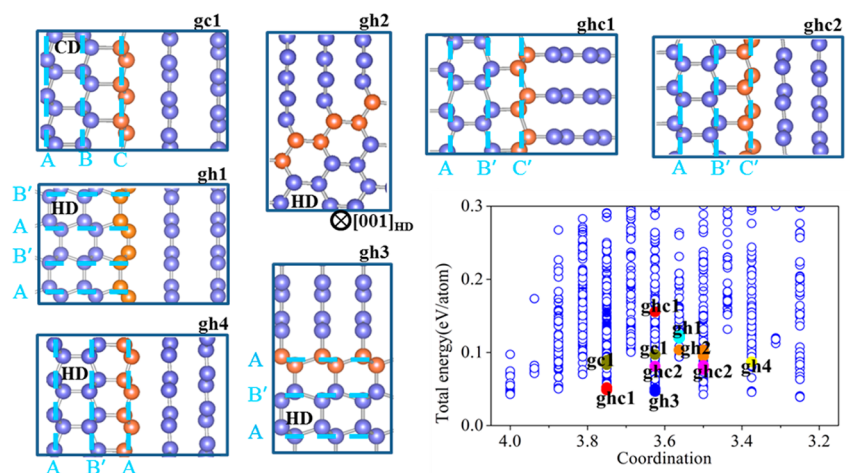
Figure 1. Finding metastable heterophase junctions from SSW global PES exploration under 15 GPa. The right-bottom figure plots energy against average coordination number of 4000 structures. Different structures could have the same interface. (gh1)-to-(ghc2) show the structure of seven most stable interfaces from DFT. The dashed lines mark the close-packed planes, i.e., (111) for CD and (001) for HD. For gh2 interface, the interface is normal with $(001)_{HD}$. The interface atoms are orange colored for clarity.

atom above graphite). As shown in Figure 1, we have plotted the energetics of the phases against the average carbon coordination number (N_c) in Figure 1 (N_c is calculated by counting the first neighbors, where the C−C distance below 1.70 Å is regarded as bonding; N_c for diamond and graphite is 4 and 3, respectively). It shows clearly that a large number of mixed phase intermediates (N_c in between 3 and 4) are obtained from SSW global structure search. By inspecting the geometry of all these structures closely, we can screen out the metastable heterophase junctions that contain graphite component, and distinguish them according to the interface type and crystallographic orientation relationships (OR). There are seven types low energy heterophase junctions as indexed from gc1 to ghc2 in Figure 1, and their associated interfaces are listed in Table 1.

Table 1. Structure and Energetics of Metastable Heterophase Junctions in Graphite-to-Diamond Solid Phase Transition

name	interface	OR	γ	ΔS	E_a
gc1	$(001)_G//(111)_{CD}$	1	0.41	−3.7%	0.79
gh1	$(001)_G//(100)_{HD}$	3	0.23	0.7%	0.47
gh2	$(110)_G//(1\bar{1}0)_{HD}$	3	0.24	22.6%	0.55
gh3	$(100)_G//(001)_{HD}$	3	0.35	25.2%	0.87
gh4	$(001)_G//(001)_{HD}$	4	0.42	−2.6%	0.85
ghc1	$(100)_G//(111)_{CD}$ $(100)_G//(001)_{HD}$	2,3		23.8%	0.84
ghc2	$(001)_G//(111)_{CD}$ $(001)_G//(001)_{HD}$	1,4		−3.2%	0.80

[a]Listed data include interface planes, crystallographic OR, interfacial energy (γ, eV/Å^2), reaction barrier (E_a, eV per interface atom) for heterogeneous pathway mediated by the corresponding junction, the area misfit between connecting phases at the interface (ΔS, with respect to graphite)

For these heterophase junctions, gc1 is the only G/CD biphase junction; gh1 to gh4 are G/HD biphase junctions differing by the interfaces; and ghc1 and ghc2 are G/HD/CD three-phase junctions. HD/CD structure can be considered as a diamond structure with stacking faults on the close-packed plane. They belong to four distinct ORs as follows:

OR1: $(001)_G//(111)_{CD}$, $[100]_G//[110]_{CD}$;
OR2: $(001)_G//(211)_{CD}$, $[100]_G//[110]_{CD}$;

OR3: $(001)_G//(100)_{HD}$, $[1\bar{1}0]_G//[001]_{HD}$;
OR4: $(001)_G//(001)_{HD}$, $[010]_G//[010]_{HD}$.

Among them, OR2 is 30° off OR1, and OR4 is 90° off OR3; OR2 does not occur independently but combines with OR3 to yield a C1-type three-phase junction.[11] We note that only OR1 and OR3 were reported in experiment previously.[4−6] For example, Britun et al. observed CD formation at 7 GPa and 1500 °C with OR1.[6]

The stability of the biphase interfaces can be assessed by the interfacial energy γ that is computable from first principles.[20] We have constructed and optimized all five biphase junctions (gc1 to gh4) in supercells using dispersion corrected density functional theory (DFT-D3) calculations,[21] as implemented in plane-wave VASP code.[22] Table 1 listed the calculated γ of the interfaces using $\gamma = (E_{X/Y} − E_X − E_Y)/2S$, where $E_{X/Y}$ is the DFT total energy of the biphase junction in a 32-atom superlattice with equal concentration for each individual phase (see SI for structures), $E_{X(Y)}$ are the total energies of pure phases and S is the area of the interface.

Table 1 shows that the gh1 and gh2 interfaces, both belonging to G/HD junctions with OR3, are two most stable interfaces with γ of 0.23−0.24 eV/Å^2. The gh3 interface, also complying with OR3, is less stable than gh1 and gh2 but more stable than others. By contrast, the only G/CD interface, gc1, is energetically much poorer with γ being 0.41 eV/Å^2, which almost reaches to the least stable G/HD interface, gh4 (0.42 eV/Å^2), whose OR (OR4) was never observed in experiment. We emphasize that the stability of these interfaces is tightly related to the strain at the biphase interface as measured by the interface energy γ, which develops at the directions both perpendicular and parallel to the interface. Because the two kinds of structural misfit couple with each other through local structural relaxation, the interface area misfit ΔS that is parallel to the interface can be utilized as a quick guide to find the best interface. For the interfaces that are parallel with the graphite (001) basal plane, including gc1, gh1 and gh4, the most stable gh1 junction corresponds to the one with the lowest lattice mismatch (e.g., 0.7% in ΔS). The same is true for the interface perpendicular to the basal plane, including gh2, gh3: the most stable gh2 junction does have the best lattice match (ΔS = 22.6%, to compare with 25.2% of gh3). The larger lattice mismatch of gh2

and gh3 is caused apparently by the large compression of graphite layers to fit into the interface (see Figure 1).

To understand the interface stability quantitatively, one need to compare the strain developed at different crystallographic directions. We have computed the uniaxial strain v.s. strain energy curve for bulk G, CD and HD, where the strain directions are taken as those in the junction gc1, gh1 and gh4. The strain energy is defined by the DFT total energy difference with and without the uniaxial stretch/compression. For gc1, gh1 and gh4 junctions, the structure misfit occurs mainly at the direction perpendicular to the interface, including [111] for CD, [100] and [001] for HD, [001] for G (Table 1). The results are presented in Figure 2. Not surprisingly, we find that the strain energy of
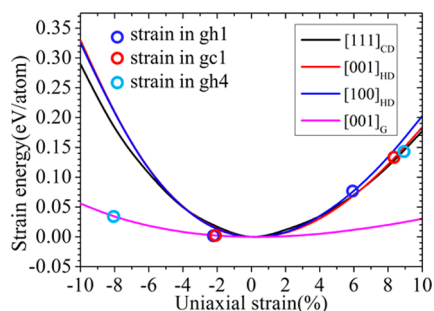

Figure 2. Strain energy vs uniaxial strain curves for bulk G, HD and CD at the vertical directions to the interface gc1, gh1 and gh4. The actual strains of G, HD and CD in the junctions are indicated by hollow circles. The larger strain is induced on the diamond side, i.e., 5.88%, 8.37% and 8.90% for diamond in gh1, gh4 and gc1 junctions, respectively.

diamond is the main contributor to the total strain energy at the interface (graphite is highly flexible at $[001]_G$). The lattice misfit for G and HD in gh1 is obviously lower than those in gc1 and gh4, and therefore the strain energy of gh1 is much smaller than those of gc1 and gh4 (see Figure 2). For a 32-atom superlattice with half−half diamond and graphite, this would lead to the total strain energies of gc1 (0.25 eV/Å^2) and gh4 (0.27 eV/ Å^2) per interface area being ∼0.11 eV/ Å^2 larger than that of gh1 (0.15 eV/Å^2), which explains that the interfacial energies of gc1 and gh4 are about 0.17 eV/Å^2 larger than that of gh1. This indicates that the stability of nascent diamond nuclei is largely determined by the strain energy induced by the lattice mismatch between graphite and diamond.

The presence of multiple metastable heterophase junctions indicates that the kinetics of the pressure-induced graphite transformation is complex, governed by multiple anisotropic reaction channels. To determine the kinetics, it is essential to identify these heterogeneous phase transition pathways as mediated by these heterophase junctions. For this purpose, we applied the recently developed SSW reaction pathway sampling to explore the low energy pathways starting from the heterophase junctions in Table 1. These pathways lead to G, HD and CD phases, and by joining the segmented pathways, we can complete the pathways linking G to different products, where the metastable heterophase junctions act as the intermediates.

The SSW reaction pathway sampling combines the SSW global structure search and the fast pathway connection tool, the variable-cell double-ended surface walking (VC-DESW) method.[23] The SSW sampling collects the likely pathways linking structural minima by recording the possible reaction coordinates, and the VC-DESW is then utilized to locate exactly the TS of solid phase transition (a saddle point on PES with one and only one

imaginary mode that is spanned by the lattice and atom degrees of freedoms) and determine the barrier of all possible pathways.

Our SSW pathway sampling starts from a chosen heterophase junction (gc1−ghc2 in Table 1), defined as initial state (IS), and then explores exhaustively the likely phases nearby (>2000 minima), defined as final state (FS). EDIP was used for carbon potential in SSW pathway sampling. After collecting a significant number of IS/FS pairs, i.e., >200 pairs for each heterophase junction, we utilize VC-DESW to locate the TS explicitly between IS and FS using DFT, based on which the low energy pathways are determined by sorting the computed barriers (also see SI).

Following the above procedure, we have determined all the lowest energy pathways mediated by the gc1−ghc2 seven different junctions and the overall barriers of them (the highest energy TS along the pathway with respect to the graphite) are listed in Table 1. It is interesting to find that gh1-pathway (via gh1 junction) and gh2-pathway (via gh2 junctions) have the lowest barrier, 0.47 and 0.55 eV per interface atom (eV/int), which is in line with the higher stability of their interfaces. The other pathways with less stable interfaces have much higher barriers, 0.75−0.90 eV/int.

In Figure 3, we present the reaction energy profiles of the lowest energy pathways mediated by gc1-, gh1- and gh4-type interfaces,
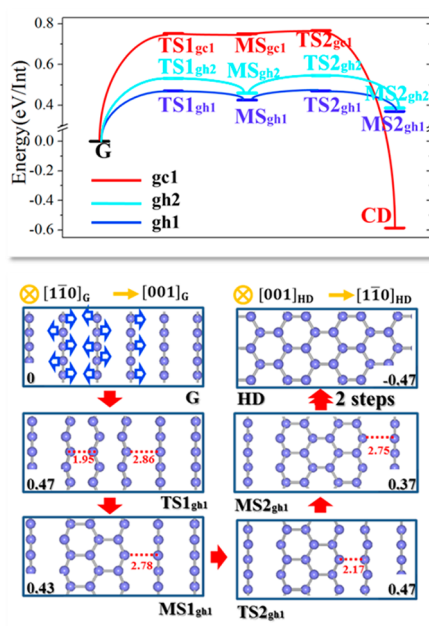

Figure 3. Reaction energy profile for three lowest energy pathways (top), and reaction snapshots along the lowest energy pathway from G to HD mediated by gh1-type interface (bottom). Relative energy of state (eV per interface atom) is indicated in the corner.

and also the reaction snapshots for the gh1 pathway. It shows that for the gh1 pathway from G to HD, it involves two intermediate states MS1 and MS2, both containing gh1-type interface. The lower overall barrier in gh1 compared to gc1 and gh4 can be attributed to the high stability of the reaction intermediates. Taking gh1 pathway as an example, we illustrate how atoms move during the phase transition microscopically (other pathways are provided in SI Figure S2). The phase transition initiates via the relative slipping of graphite basal plane along $[1\bar{1}0]_G$ by 1/2 C−C length (0.7 Å) followed by the compression at $[001]_G$. From G-to-MS1, the first step, the compression leads to the buckling of three neighboring graphite layers. The neighboring carbon rows along

$[1\bar{1}0]_G$ in a graphite layer then displace collectively out of the basal plane at opposite directions and approach to the neighboring graphite layers. New C−C bonds are evolved at the TS (TS1$_{gh1}$) is 1.95 Å, after which a three-atomic-layer HD nucleus is created at MS1, showing the characteristic sp^3 bonding of diamond. The remaining steps, MS1-to-MS2 and MS2-to-HD, propagate the interface at $[001]_G$ with the same atom displacement pattern, leading to the growth of HD phase. The graphite basal plane evolves into $(100)_{HD}$, accompanied by 25.6% compression at $[001]_G$. In the pathway, the stability of the nascent HD nucleus (MS1) in graphite matrix dictates largely the barrier height (TS1) of transformation, demonstrating the critical role of nucleation in kinetics.

By analyzing these anisotropic transition pathways mediated by different interfaces, we identify two general features: (i) All pathways require a significant compression perpendicular to $(001)_G$ no matter the interface type. Due to the large d-spacing of $(001)_G$, the $[001]_G$ compression is generally very large (at least 20.3%) for all pathways. As discussed in Figure 2, the magnitude of $[001]_G$ compression in graphite is however not the determining factor for kinetics. Instead, the strain in diamond phase dominates the energy cost to form heterophase junction; (ii) The initial step of nucleation can be regarded as the rate controlling step, where the barrier to form nascent nucleus is equal or very close to the overall barrier of the whole transition (see Figure 3 and S2). This points out the importance of nuclei formation, which creates the first heterophase junctions between graphite and diamond.

The rate for graphite phase transition following heterogeneous pathways can be estimated: the formation of CD phase is at least 40 times slower compared to that to form HD phase at 1000 °C from microkinetics (by assuming the same prefactor). On the other hand, the reactions to CD phase and other mixed phase microstructures occur simultaneously: the rate difference is less than 1.12 times at 1000 °C. These quantities confirm HD phase is kinetically much favored, which correct the wrong prediction from collective pathways and MD results.[8−11] Indeed, the G/HD composite with OR3 were commonly observed at 1000 °C,[4−6] where CD phase is not formed yet; Németh et al. observed the mixed phase (CD/HD) at 2200 °C and 19 GPa[7] using transmission electron microscopy, indicating that the high temperature is a must to overcome the barrier of CD nucleation. We attribute the high HD selectivity to the presence of three low energy G/HD junctions, i.e., gh1, gh2 and gh3, orthogonal with each other, and two low energy anisotropic pathways via gh1 and gh2 junctions. These maximally stabilize HD nuclei inside graphite and allow for HD propagation in three dimensions (3D). By contrast, there is only one and high barrier gc1-pathway to form CD. Its barrier is similar to the pathways leading to the mixed phases (Figure 3). This indicates that the nascent CD nuclei in 3D inevitably introduce incoherent interfaces inside graphite and thus the CD growth is not favored both thermodynamically and kinetically.

To recap, using the SSW global optimization method to search for low energy heterophase interfaces, we reveal that the nucleation core of HD phase is coherent in 3D with G matrix, but that of CD is semicoherent with only one likely coherent interface. Because of the interface strain, the barrier to diamond nucleation/growth is generally much lower for HD phase, rationalizing for the first time that the preferable product from compressed graphite at 15 GPa is metastable HD instead of CD. The theoretical approaches utilized and the understanding achieved are expected to be applicable generally for solving the nucleation kinetics in other diffusionless solid transitions.

■ ASSOCIATED CONTENT

ⓈSupporting Information

The Supporting Information is available free of charge on the ACS Publications website at DOI: 10.1021/jacs.6b11193.

Experimental details (PDF)

■ AUTHOR INFORMATION

Corresponding Author

*zpliu@fudan.edu.cn

ORCID ⓘ

Zhi-Pan Liu: 0000-0002-2906-5217

Notes

The authors declare no competing financial interest.

■ ACKNOWLEDGMENTS

■ REFERENCES

(1) DeCarli, P. S.; Jamieson, J. C. *Science* **1961**, *133*, 1821−1822.

(2) Hanneman, R. E.; Strong, H. M.; Bundy, F. P. *Science* **1967**, *155*, 995−997.

(3) Naka, S.; Horii, K.; Takeda, Y.; Hanawa, T. *Nature* **1976**, *259*, 38−39.

(4) Bundy, F. P.; Kasper, J. S. *J. Chem. Phys.* **1967**, *46*, 3437−3446.

(5) Yagi, T.; Utsumi, W.; Yamakata, M.-a.; Kikegawa, T.; Shimomura, O. *Phys. Rev. B: Condens. Matter Mater. Phys.* **1992**, *46*, 6031−6039.

(6) Britun, V. F.; Kurdyumov, A. V.; Petrusha, I. A. *Powder Metall. Met. Ceram.* **2004**, *43*, 87−93.

(7) Németh, P.; Garvie, L. A. J.; Aoki, T.; Dubrovinskaia, N.; Dubrovinsky, L.; Buseck, P. R. *Nat. Commun.* **2014**, *5*, 5447.

(8) Fahy, S.; Louie, S. G.; Cohen, M. L. *Phys. Rev. B: Condens. Matter Mater. Phys.* **1987**, *35*, 7623−7626.

(9) Tateyama, Y.; Ogitsu, T.; Kusakabe, K.; Tsuneyuki, S. *Phys. Rev. B: Condens. Matter Mater. Phys.* **1996**, *54*, 14994−15001.

(10) Khaliullin, R. Z.; Eshet, H.; Kühne, T. D.; Behler, J.; Parrinello, M. *Nat. Mater.* **2011**, *10*, 693−697.

(11) Scandolo, S.; Bernasconi, M.; Chiarotti, G. L.; Focher, P.; Tosatti, E. *Phys. Rev. Lett.* **1995**, *74*, 4015−4018.

(12) Xiao, P.; Henkelman, G. *J. Chem. Phys.* **2012**, *137*, 101101.

(13) Mujica, A.; Rubio, A.; Muñoz, A.; Needs, R. J. *Rev. Mod. Phys.* **2003**, *75*, 863−912.

(14) Erskine, D. J.; Nellis, W. J. *Nature* **1991**, *349*, 317−319.

(15) Wang, J.-T.; Chen, C.; Kawazoe, Y. *Phys. Rev. Lett.* **2011**, *106*, 075501.

(16) Shang, C.; Liu, Z.-P. *J. Chem. Theory Comput.* **2013**, *9*, 1838−1845.

(17) Shang, C.; Zhang, X.-J.; Liu, Z.-P. *Phys. Chem. Chem. Phys.* **2014**, *16*, 17845−17856.

(18) Guan, S.-H.; Zhang, X.-J.; Liu, Z.-P. *J. Am. Chem. Soc.* **2015**, *137*, 8010−8013.

(19) Marks, N. A. *Phys. Rev. B: Condens. Matter Mater. Phys.* **2000**, *63*, 035401.

(20) Zhao, W.-N.; Zhu, S.-C.; Li, Y.-F.; Liu, Z.-P. *Chem. Sci.* **2015**, *6*, 3483−3494.

(21) Grimme, S.; Antony, J.; Ehrlich, S.; Krieg, H. *J. Chem. Phys.* **2010**, *132*, 154104.

(22) Kresse, G.; Furthmüller, J. *Phys. Rev. B: Condens. Matter Mater. Phys.* **1996**, *54*, 11169−11186.

(23) Zhang, X.-J.; Liu, Z.-P. *J. Chem. Theory Comput.* **2015**, *11*, 4885−4894.